Journal of Manufacturing Processes 58 (2020) 208–222

Contents lists available at ScienceDirect

Journal of Manufacturing Processes

journal homepage: www.elsevier.com/locate/manpro

Technical Paper

Combination of high feed turning with cryogenic cooling on Haynes 263 and Inconel 718 superalloys

F.J. Amigo[a], G. Urbikain[b,*], O. Pereira[a], P. Fernández-Lucio[a], A. Fernández-Valdivielso[a], L.N. López de Lacalle[a]

[a] CFAA, Department of Mechanical Engineering, University of the Basque Country, Faculty of Engineering of Bilbao, Alameda de Urquijo s/n, 48013, Bilbao, Spain
[b] CFAA, Department of Mechanical Engineering, University of the Basque Country, Faculty of Engineering of Gipuzkoa, Plaza Europa 1, 20018, Donostia-San Sebastián, Spain

ARTICLE INFO

Keywords:
high feed
force model
aerospace superalloys
cryogenic turning

ABSTRACT

The machining of heat resistant superalloys (HRSA) is one of the most challenging tasks for machinists. Unfortunately, the turning of these difficult-to-cut materials is very common in the manufacturing of cases for gas turbines components due to their excellent mechanical properties. Traditionally, these operations are very time consuming. In order to avoid failure and part rejection, very conservative cutting parameters are selected; so, there is a great margin to optimize cutting conditions in aerospace applications. Besides, the minimization or avoidance of coolant is day-to-day a shared practice. All these factors make the turning of HRSA a very complex problem.

Lately, high-feed turning technique has emerged as an alternative to traditional turning for a faster, more productive, manufacturing. It is based on moving the tool from the jaws towards the tailstock in reverse mode with a very low side cutting edge angle. It is a promising process but rather unknown. This paper presents an experimental investigation of the cutting forces and their prediction in high feed turning of Nickel-Chrome based superalloys. Besides, the effects of using oil emulsion and CO_2 cryogenic coolant were also studied. Straight turning tests on different aerospace materials, Inconel 718 and Haynes 263, were compared against AISI 1055, using comparable cutting conditions. After the tests, surface roughness was also examined with both types coolants.

The results indicated a good agreement between model predictions and experimental results for the three tested materials. It was also shown that while oil emulsion was the best option for Inconel 718, cryogenic cooling with CO_2 can open the path towards a more efficient and cleaner turning in the case of Haynes 263.

1. Introduction

Manufacturing of aerospace components is always a critical issue for aircraft part suppliers. Indeed, these parts collect some special circumstances that harshly constraint production times. First, the tight tolerances requested by aerospace industry that force any new machining alternative to be verified and regulated before use. This is even truer for rotating elements. Besides, some parts of the gas turbine are challenging environments where temperatures and pressures are beyond the limits of most of metals. For parts such as cases, shafts or wheels, heat resistant super alloys (HRSA) are suitable due to their exceptional property retention (mechanical, corrosion and creep resistance) at temperatures between 650-850 °C [1].

HRSA are also catalogued as difficult to cut or low machinability materials. The reasons for this poor machining are behind their benefits as withstanding materials. Several parameters lead to accelerated tool wear: (1) exceptional resistance maintained at high temperatures, (2) highly abrasive carbide particles within the microstructure, (3) low thermal conductivity, (4) high chemical affinity [2]. These issues combined with the high competitiveness from aeronautical sector imply the need of improving the machining processes, mainly in rough turning operations of rotary parts such as turbine disks in which “takt times” have to be reduced drastically. So, optimizing cutting parameters is an important piece of the puzzle. Besides, a good balance needs to be found with the mechanical stresses produced on turning inserts.

As mentioned, one of the lines for optimizing cutting parameters is the previous estimation of the mechanical stresses before machining the

* Corresponding author.
E-mail address: gorka.urbikain@ehu.eus (G. Urbikain).

https://doi.org/10.1016/j.jmapro.2020.08.029
Received 13 February 2020; Received in revised form 9 July 2020; Accepted 12 August 2020
Available online 18 August 2020
1526-6125/

workpiece. For example, Sadilek et al. [3] investigated the effect of depth of cut on cutting forces, identifying the problems that may occur when varying this parameter. They compared cutting forces and tool wear between a standard roughing cycle and their own-developed one. Results showed that a variable roughing cycle lead to a more favorable distribution of tool wear, being tool life extended by 44%. Simultaneously, there was a decrease in spindle load of about 10%. Selaimia et al. [4] also proposed an interesting study on depth of cut. In this case, besides cutting force (*Fc*), cutting power (*Pc*), specific cutting force (*Ks*) and material removal rate (*MRR*) were taken into account. They concluded that the depth of cut was the predominant parameter on the cutting force and cutting power, whereas feed per tooth is the most important factor affecting surface roughness and the specific cutting force.

The results from some research works focused on milling can also be extrapolated to turning process due to orthogonal cutting hypothesis was assumed. Among them, Tukora and Szalai [5] introduced a cutting force estimation procedure based on a mechanistic cutting force model without limiting the geometry of the cutting tool. Matsumura and Tamura [6] determined the chip flow direction by minimizing cutting energy. These authors assumed a three-dimensional chip flow as a piling up of the orthogonal cutting in the planes containing the cutting velocities and the chip flow velocities. Tsai et al. [7] presented two approaches for cutting force estimation. The first one was based on the work from Altintas [8], while the other one was based on the Recursive Smallest Square (RLS) method. In both cases, results were compared with the experimental values and a good agreement was found between the RLS method and the experimental values. Despite being useful in their application fields, all these research works were limited to conventional cutting conditions and so, cannot be easily extrapolated to HRSA applications, where workpiece materials meet high hardness and ductility.

In this line, several research works were devoted to high speed turning and Nickel-based HRSA. Zhou et al. [9] compared the behavior of AD730 Nickel-based alloy and Inconel 718 under high speed turning with PCBN tools. The results showed that cutting forces were about 10% lower compared with Inconel 718, with cutting speeds up to 350 m/min in both materials. Denkena et al. [10] also used PCBN inserts for the high speed turning of Inconel 718. Specifically, they prepared the inserts using pulsed laser ablation (PLA) with a nanosecond pulsed laser. The preparation was divided into two steps where laser was oriented perpendicular to the flank and rake faces and gave lower cutting forces thanks to a lower chip/insert contact. Chen et al. [11] obtained a balance between machining efficiency and surface integrity when using PCBN between 200-250 m/min in turning AD730. Soo et al. demonstrated [12] that the use of TiSiN coating in PCBN inserts lead to increased tool life (+40%) with respect to uncoated inserts. They used cutting speeds of 200 m/min in the turning of Inconel 718. Tian et al. [13] used the high speed turning technique. In this case, a ceramic tool based on Si3N4 was applied to iron-based GH2132 HRSA at cutting speeds up to 200 m/min. They observed that cutting forces were reduced gradually with the cutting temperature increase. All these works share the objective of reducing cutting times in the machining of HRSA by using advanced tools such as PCBN or ceramic substrates. This implies an increase of tool costs that has effects on competitiveness.

Due to their specific problematics, HRSA represent a vast niche for experimental works. Yilmaz et al. [14] developed an original chip-breaking system based on a gearbox design to improve chip evacuation when turning Inconel 718. Their system resulted in reduced cutting forces and better surface finish. Suarez et al. [15] compared the machinability of Haynes 28 at aged and solutioned state. They observed the strong influence of the work history on machinability and wear mechanisms: flank and notch wear were primarily identified to aged state and crater wear for solutioned state. Recently, Gunay et al. [16] analyzed tool life in the turning of difficult-to-cut Nimonic 80A. These authors applied different cooling conditions - dry, air-cooling and oil-spraying – and studied tool performance by SEM and EDS characterization. They used response surface method to find the optimum cutting speed at 60 m/min. In most cases, the cutting speeds remain between 60-90 m/min [17,18], that is, the half of the obtained with advanced substrates. Then, the way of obtaining a reduction of the cutting times has to be focused from another point of view in which carbide tools (WC) can be used.

Under this perspective, high-feed turning is presented as an alternative to the increase of cutting speed. It is based on reducing the position angle of the insert. The engaged cutting edge is increased, chips become thinner, and therefore, wear is expected to be reduced as well as cutting forces per unit of edge length [19]. With the aim of doubling feed without affecting surface roughness, tool tip radius can also be changed if using wiper inserts [20]. Some authors achieved improved feed rates [21,22] in C45 and AISI D2 steels, respectively. However, this technique has not yet been studied with HRSA materials, which are of special interest. Indeed, for such materials, increasing productivity is highly limited with tool costs. So, a balance must be met.

To complete the whole picture of the challenge HRSA machining does represent, environmental issues are becoming also a major constraint for aerospace industry. An increase in productivity needs to be accompanied by a reduction in the environmental footprint, because society is becoming more aware about global warming and demands more ecological industrial practices. In machining operations, the elimination of cutting fluids is the focus point. In this line, cryogenic machining was lately presented as a feasible solution. In particular, several alternatives to oil emulsions were studied by authors previously [23]. Among them, CO_2-CryoMQL machining was proposed: oil flowrates are reduced drastically while similar tool life can be achieved in comparison with oil emulsions. This is the case for Inconel 718 and milling processes, where the tool life is only reduced by 6,5% in comparison with oil emulsions [24]. Behera et al. [25] conducted an interesting experimental study on lubricoolant strategies (High-pressure jet, cryogenic, minimum quantity lubrication and minimum quantity lubrication with nanofluid). They characterized flank wear and surface finish and determined the cryogenic technique as the best option for the machining of Inconel 718. Specially in turning, the possibility of using CO_2 in stand-alone mode is interesting as it is inherently a more stable process compared to milling. The results obtained by LN_2 cryogenic cooling were satisfactory. This line was studied deeply in [26] in which Inconel 718 and Ti6Al4V were turned, respectively. In this research, it was concluded that, with these alloys, the use of LN_2 implied a tool life increase in comparison with oil emulsions. Besides, it was also observed the effectiveness of cryogenic gases on the work pressure rather than on the flow rate. From an industrial point of view, CO_2 is more attractive than LN_2 due to LN_2 storage problems [27]. Besides, CO_2 is injected at higher pressures than LN_2, what implies a better penetration in the tool-chip interface. So, studying the CO_2 behavior in heat thermoresistant alloys is a need in order to satisfy both, societal and industrial issues. It should be noted that CO_2 can be recycled, this is, it captured from a primary process, liquified and used as cutting fluid, then, environmental innocuousness associated to LN_2 cryogenic cooling is maintained. From this point of view, using CO_2 as cutting fluid to control cutting temperature and allow higher feed rates is an interesting line to be analyzed.

In this paper, the capabilities of the high feed turning were investigated for applications involving low machinability materials. In order to investigate cooling alternatives and their feasibility on this turning operation, the effects of oil emulsion and CO_2 coolant and cutting parameters on cutting forces and surface roughness were also verified. Section 2 presents the fundamentals on the new developed high-feed turning concept. Section 3 describes some trends observed regarding cutting force and roughness measurements, cryogenic techniques and tested materials. Section 4 describes the mechanistic model

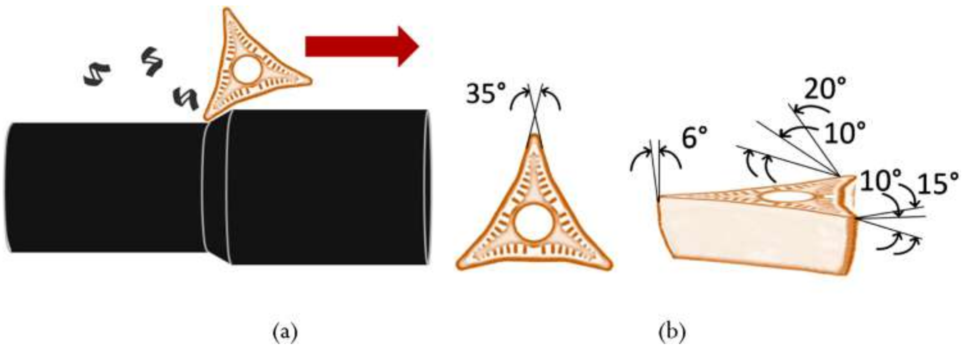

Fig. 1. a. High feed turning (Prime Turning©); b. Insert A-type (view of basic side cutting edge angle, rake angle, secondary angles for chip breakage).

and the cutting coefficients calibration, as well as a discussion of the results obtained. Section 5 presents the agreement between simulated values and experimental ones. Finally, some conclusions are drawn.

2. High-feed turning: the process and the tool

Recently, High-feed turning process was proposed as an alternative to common turning operations. One important feature is that the tool is engaged with the workpiece in reverse (Fig. 1a) with a low cutting-edge angle thus using a very small part of tool radius. Under Prime Turning© brand, Sandvik Coromant has developed two insert types: A-type, with three 35º vertices for roughing, finishing and profiling operations, and B-type, with resistant vertices for large roughing. In this study, the behavior of type A was explored due to its versatility, since it makes possible the rotation of flat and wall faces using both insertion edges in a single operation. Main features are: ISO code CP-A1108-L3, grade GC1115, substrate HC and coating PVD TIALN + ALCR2O3, grain size < 1 μm, HRc = 80, Fracture toughness $=8.8$ MPa·m$^{1/2}$, inscribed circle diameter iD $=11$ mm, nose radius r_ε $=0.794$ mm; insert angle = 35º, side cutting edge angle κ_r = 30º, rake angle γ = 0º. The toolholder (QS-CP-30AR-2525-11C), which is out of standard, supplies a neutral positioning which is altered by tool's chip breaker (Fig. 1b).

Fig. 2 shows cutting geometry with the usual reference systems: *z*, for the axial direction of the piece (coincident with longitudinal, feed direction) and *x*, in the workpiece radial direction. System *tra* (with t parallel to y-axis), which will be used in Section 4, is centered in the tool and rotated with respect to *xyz* the side cutting edge angle κ_r (Fig. 2a). For a depth of cut of a_p $=0.5$ mm, the evolution of the side cutting edge angle from the innermost point till the maximum depth of cut is shown (Fig. 2b) and the geometrical location of the points in the *xz* plane (Fig. 2c). For the case considered, it seems reasonable to use the constant position angle hypothesis, which is fulfilled from the depth a_p $=0.1$ mm onwards.

3. Experimental cutting tests

3.1. Work materials

Inconel 718 (UNS N07718/W.Nr. 2.4668) is one of most challenging aerospace superalloys. It belongs to the Nickel-Chromium group and widely used not only in gas turbine but also in nuclear reactors, pumps, etc. The work material was supplied in aged state, the material is hardened by precipitation of secondary phases into the metal matrix. Haynes 263 or Nimonic 263 (UNS N07263/W. Nr. 2.4650) alloy is normally used for applications up to about 900 °C. Its oxidation resistance is comparable to that for other gamma-prime-strengthened superalloys. This material is adequate for a variety of applications in the aircraft turbine engine as well as for power generation turbines. For comparison purposes, AISI 1055 steel was also included in the cutting tests as reference. This is a non-alloyed steel with a high carbon percentage of 0.55% that leads to a high resistance to wear increasing the growth of perlite phase. It is profusely used in construction and machinery manufacturing. Table 1 shows the main properties for the three materials.

3.2. Experimental set-up

To obtain the specific cutting coefficients, a set of longitudinal turning tests was designed. Table 2 shows the cutting parameters for the first characterization stage. These cutting conditions were defined upon the recommendations from toolmakers (catalogues) as well as from past experiences of the authors with that superalloys [2,27]. While cutting speed is highly dependent on work material, a shared range was set for both difficult-to-cut materials Haynes 263 and Inco718. As AISI 1055 steel is not so critical in terms of tool breakage, a different range was fixed. Depths of cut and feeds were taken in the same range because the test campaign was intended for studying finishing operations in all the materials.

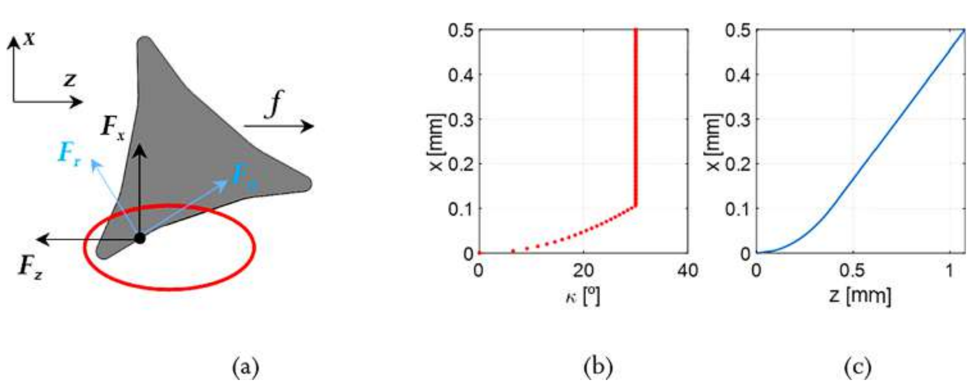

Fig. 2. a. Schematic representation of longitudinal turning; b. Evolution of side cutting edge angle with; c. Real cutting-edge profile.

Table 1
Composition and mechanical/thermal properties for the tested materials.

Materials	Chemical composition	Density [g/cm3]	Ultimate tensile strength [MPa]	Yield tensile strength [MPa]	Thermal conductivity [W/m·K]	HardnessHRc
Inconel 718	52.5%Ni, 19%Cr, 17%Fe, 5%Nb, 3%Mo, 1%Co, 1%Ti, 0.6%Al, 0.35%Mn, 0.35%Si, 0.08%C, others	8.19	1,100 at 650 °C	1,100 (strain 0.2%)	11.4	45
Haynes 263	49,6%Ni, 20%Cr, 20%Co, 6%Mo, 2%Ti, 0.7%Fe, 0.6%Al, 0.6%Mn, 0.4%Si, 0.06%C, others	8.36	835 at 650 °C	635 (strain 0.2%)	11.7	27
Steel AISI 1055	98,6%Fe, 0.75%Mn, 0.55%C, 0.05%S, 0.04%S	7.87	650	355	51.9	11

The tests were carried out in a CMZ® *Machinery Group* machining centre, model TC25BTY. Maximum spindle speed: 4000 rpm and 35 kW. The workpiece was clamped from both extremes to avoid vibrations. Two different cooling alternatives, oil emulsion and CO_2 were selected. The first fluid consisted of a synthetic oil-water emulsion *Quaker Houghton* Hocut® 4940, with a concentration of 10% and flow rate 6 l/min. As for the liquefied CO_2, it was injected at a pressure of 14 bar through a nozzle with a final diameter of 1.5 mm and −78 °C output temperature. The BeCold® control unit was used for this purpose, which ensures the stability of the fluid during injection while preventing dry ice formation through the pipes. All the tested conditions were done with new inserts, to avoid the influence of wear. Cutting forces were measured with a Kistler dynamometer (9257B) and a vibration multichannel analyzer (OROS-NVGATE). Roughness was measured in all the cases with a fresh tool. A *Taylor Hobson*® Surtronic Duo roughness tester was used. Fig. 3 shows the experimental set-up.

A comparison of the cutting forces and roughness can be raised according to the cutting parameters: $a_p = 0.5$ - 1 [mm]; $f = 0.2$ - 0.4 [mm/rev]; $V_c = 40$ - 80 [m/min] for superalloys and $V_c = 200$ - 400 [m/min] for AISI 1055. The values selected for this comparison are shown in Table 3 and are obtained by duplicating the following references: $V_c = 40$ [m/min], $f = 0.2$ mm/rev, $a_p = 0.5$ [mm]. In this way, each time only one of the parameters is doubled, the material removal rate is also doubled. For example, tests 2, 3 and 4 have the same $MRR =$ 8 [cm^3/min] (40 [cm^3/min] in the case of AISI 1055) while only one of the parameters changed with respect to test 1. In tests 5, 6 and 7, two of the parameters are modified alternately. Finally, in test 8, all three are duplicated. The same 8 tests were performed first with oil emulsion and then with CO_2 to compare the difference between the two coolants.

The results of the comparison using both types of coolants are depicted in the following sections. Sections 3.3 presents the cutting force components and Section 3.4 the average roughness, R_a, and maximum roughness, R_z, along with the expected (theoretical) values according to Shaw [28] equations ($R_z = f^2/(8r_\varepsilon)$ and $R_a = R_z/4$).

3.3. Cutting forces: materials and cooling techniques

Figs. 4, 5 and 6 allow to compare the three cartesian components obtained for a variety of cutting conditions (see Table 3). In finishing operations, the largest component is usually F_y. As can be seen, in high feed turning, the highest force component is always the passive force F_x. This is due to the small side cutting edge angle that creates a high normal component. The maximum total cutting force occur at high a_p and f but at small cutting speeds. They tend to be reduced at high V_c. So, the cutting speed has a clear influence on the forces.

In terms of work materials, both superalloys seem to have at first sight a similar behaviour, with very similar force values. The cutting forces in AISI 1055 seem to follow the same pattern but at very different scale. The forces for every component show a subtle difference between the use of emulsion and CO_2 and the use of coolant seems to be more effective at higher cutting speeds.

3.4. Roughness

Figs. 7, 8 and 9 show the surface roughness corresponding to the conditions in Table 3. The roughness values obtained and the theoretical values have been represented. As a general rule, it is observed that the roughness is higher with the use of CO_2 than with emulsion. A good correlation between actual and theoretical roughness can be observed in cases where emulsion has been used. However, this is not the case with the use of CO_2. This is clearly related to the lubricating ability of oil in the emulsion.

It is also observed the clear influence that feed rate has. In tests where f is higher, the roughness also increases, when emulsion is used. Where CO_2 is used, the feed rate dependence is important, but the other cutting parameters also influence the roughness. The poorer lubrication

Table 2
Cutting conditions for the experimental characterization.

Materials	*Vc* [m/min]	*ap* [mm]	*f* [mm/rev]	L_{BAR} [mm]	$L^{*}_{SECTION}$ [mm]	*D* [mm]
Inconel 718	40-60-80	0.3-0.5-1	0.2-0.3-0.35-0.4	275	14.67-22.0-25.67-29.33	94-60
Haynes 263	40-60-80	0.3-0.5-1	0.2-0.3-0.35-0.4	240	12.8-19.2-22.4-25.6	121-91
AISI 1055	200-300-400	0.3-0.5-1	0.2-0.3-0.35-0.4	121	6.45-9.68-11.29-12.91	109-84

* The length of each cutting section is set to fix the same time interval.

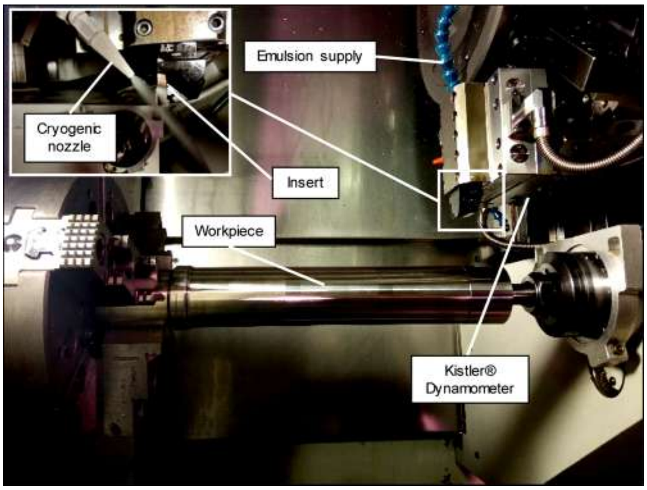

Fig. 3. Experimental set-up: workpiece, dynamometer and shank tool with internal emulsion supply and cryogenic nozzle.

and therefore the loss of contact between tool and workpiece mean that the cutting parameters have a different influence on the surface finish.

The use of CO_2 in Inconel 718 suggests a large influence of *ap* on roughness, since in general, an increase in *ap* produces an increase in roughness compared to the theoretical roughness.

The use of CO_2 in Haynes 263 shows a behaviour of the roughness more coherent with feed. The depth of cut does not seem to have a great influence. On the other hand, the cutting speed seems to be important. An increase in the cutting speed decreases the roughness at small feeds (comparison of tests 1 and 2 and comparison of tests 4 and 6). However, at higher feeds, the increase in speed is detrimental to the roughness (comparison of tests 3 and 5 and comparison of tests 7 and 8).

In the case of AISI 1055 with the use of CO_2, there is a good agreement between the measured and theoretical roughness as far as the feed is concerned. However, in all cases where the a_p increases, the roughness increases, specially, in small feeds. On the other hand, all cases where V_c increases, the roughness decreases.

The roughness behaviour with cryogenic contribution is closely related to the hardness of the material since, in general, the roughness is the highest in Inconel 718 and the lowest in AISI 1055. In Inconel 718 the increase in a_p increases the roughness, probably due to the existence of resistant crests while the feed and the cutting speed do not have such an influence. In AISI 1055, the increase in a_p also has an effect on the roughness, especially at small feeds. Increasing the cutting speed decreases the roughness and as for the feed, the roughness and the theoretical roughness are closely related. In the case of Haynes 263, the roughness depends on intermediate conditions, there is a certain relationship with the theoretical roughness in terms of feed, although lower than with AISI 1055, and cutting speed is favourable only in some cases.

4. High-feed turning model

4.1. Cutting force model

For the prediction of cutting forces, the followed approached is based on traditional mechanistic models from Altintas and Budak

Table 3
Cutting conditions for the comparison of force and surface roughness.

Test number	1	2	3	4	5	6	7	8	Material
***Vc* [m/min]**	40	80	40	40	80	80	40	80	Superalloys
	200	400	200	200	400	400	200	400	AISI 1055
***f* [mm/rev]**	0.2	0.2	0.4	0.2	0.4	0.2	0.4	0.4	Superalloys / AISI 1055
a_p [mm]	0.5	0.5	0.5	1	0.5	1	1	1	Superalloys / AISI 1055
***MRR* [cm^3/min]**	4	8	8	8	16	16	16	32	Superalloys
	20	40	40	40	80	80	80	160	AISI 1055

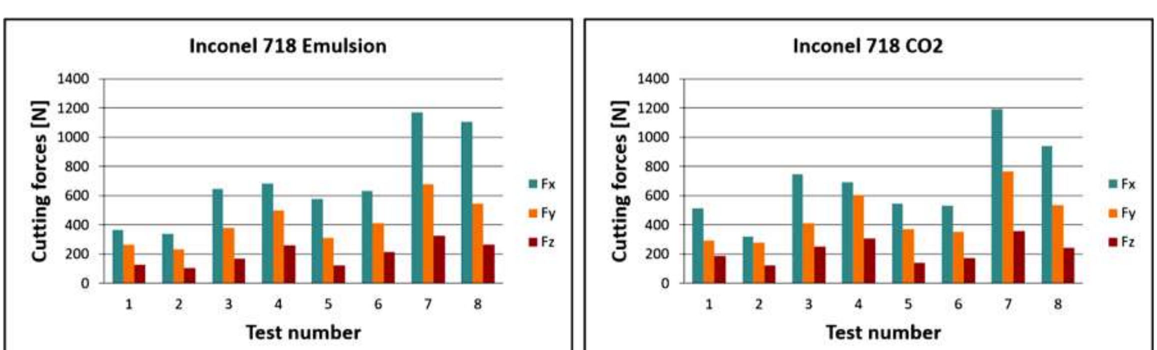

Fig. 4. Cutting forces (Inconel 718, emulsion and CO_2 conditions).

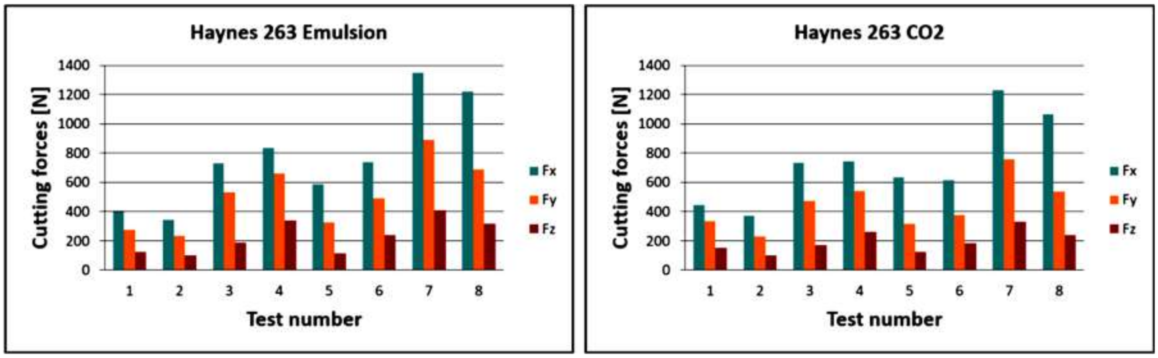

Fig. 5. Cutting forces (Haynes 263, emulsion and CO_2 conditions).

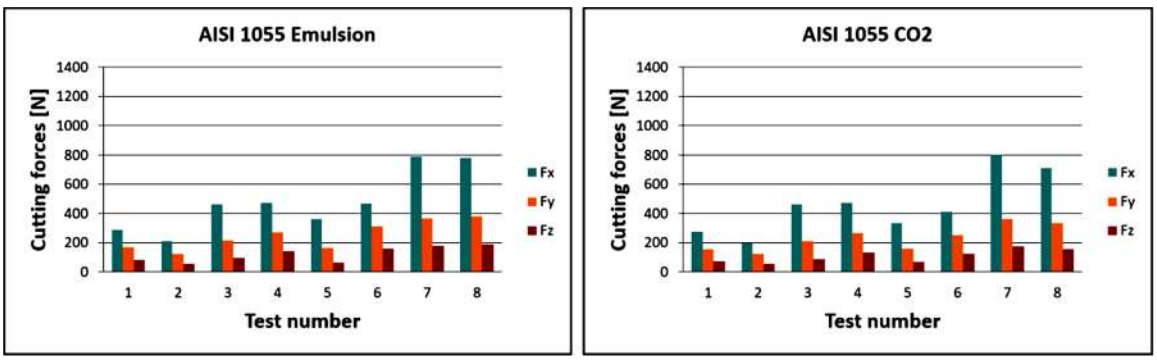

Fig. 6. Cutting forces (AISI 1055, emulsion and CO_2 conditions).

[8,29]. The key for their success is that they represent cutting mechanics in a fast and intuitive way. For a cutting tool having a constant approach angle κ_r, as the case offered by A-type inserts for high feed turning, the cutting forces in the *xyz* system can be express in function of system *tra* (Fig. 2a):

$$\begin{Bmatrix} F_x \\ F_y \\ F_z \end{Bmatrix} = [A]\cdot\begin{Bmatrix} F_r \\ F_t \\ F_a \end{Bmatrix} = \begin{bmatrix} \cos\kappa_r & 0 & \sin\kappa_r \\ 0 & 1 & 0 \\ \sin\kappa_r & 0 & -\cos\kappa_r \end{bmatrix}\cdot\begin{Bmatrix} F_r \\ F_t \\ F_a \end{Bmatrix} \tag{1}$$

where *Fr*, *Ft* and *Fa* are expressed in function of cutting parameters a_p and f as:

$$\begin{Bmatrix} F_r \\ F_t \\ F_a \end{Bmatrix} = \begin{Bmatrix} K_{rc}\cdot f\cdot a_p + K_{re}\cdot a_p \\ K_{tc}\cdot f\cdot a_p + K_{te}\cdot a_p \\ K_{ac}\cdot f\cdot a_p + K_{ae}\cdot a_p \end{Bmatrix} \tag{2}$$

where coefficients K_{rc}, K_{tc}, K_{ac} and K_{re}, K_{te}, K_{ae} account, respectively, for shear cutting and edge-friction effects. So, the final system turns into:

$$\begin{Bmatrix} F_x \\ F_y \\ F_z \end{Bmatrix} = \begin{Bmatrix} \cos\kappa_r\,(K_{rc}\cdot f\cdot a_p + K_{re}\cdot a_p) + \sin\kappa_r\,(K_{ac}\cdot f\cdot a_p + K_{ae}\cdot a_p) \\ K_{tc}\cdot f\cdot a_p + K_{te}\cdot a_p \\ \sin\kappa_r\,(K_{rc}\cdot f\cdot a_p + K_{re}\cdot a_p) - \cos\kappa_r\,(K_{ac}\cdot f\cdot a_p + K_{ae}\cdot a_p) \end{Bmatrix} \tag{3}$$

4.2. Calculation of specific cutting coefficients

From the measurements of the experimental forces in *xyz*, different systems are built and solved for each cutting speed and each depth of cut. For 6 different unknowns a minimum of two feeds are necessary:

$$inv[A]\begin{Bmatrix} F_{x,f_1} \\ F_{y,f_1} \\ F_{z,f_1} \\ F_{x,f_2} \\ F_{y,f_2} \\ F_{z,f_2} \end{Bmatrix}_{a_p,V_c} = \begin{Bmatrix} F_{r,f_1} \\ F_{t,f_1} \\ F_{a,f_1} \\ F_{r,f_2} \\ F_{t,f_2} \\ F_{a,f_2} \end{Bmatrix}_{a_p,V_c} = \begin{bmatrix} f_1\cdot a_p & a_p & 0 & 0 & 0 & 0 \\ 0 & 0 & f_1\cdot a_p & 0 & 0 & 0 \\ 0 & 0 & 0 & 0 & f_1\cdot a_p & a_p \\ f_2\cdot a_p & a_p & 0 & 0 & 0 & 0 \\ 0 & 0 & f_2\cdot a_p & a_p & 0 & 0 \\ 0 & 0 & 0 & 0 & f_2\cdot a_p & a_p \end{bmatrix}\begin{Bmatrix} K_{rc} \\ K_{re} \\ K_{tc} \\ K_{te} \\ K_{ac} \\ K_{ae} \end{Bmatrix} \tag{4}$$

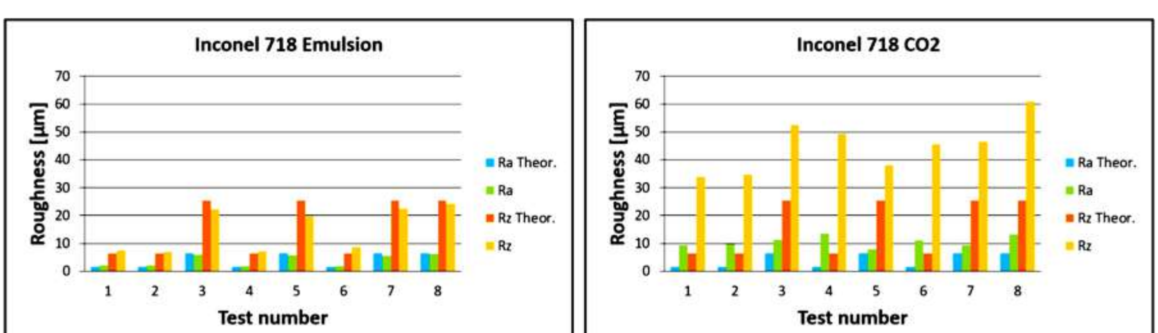

Fig. 7. Measured and theoretical roughness R_a, R_z (Inconel 718, emulsion and CO_2 conditions).

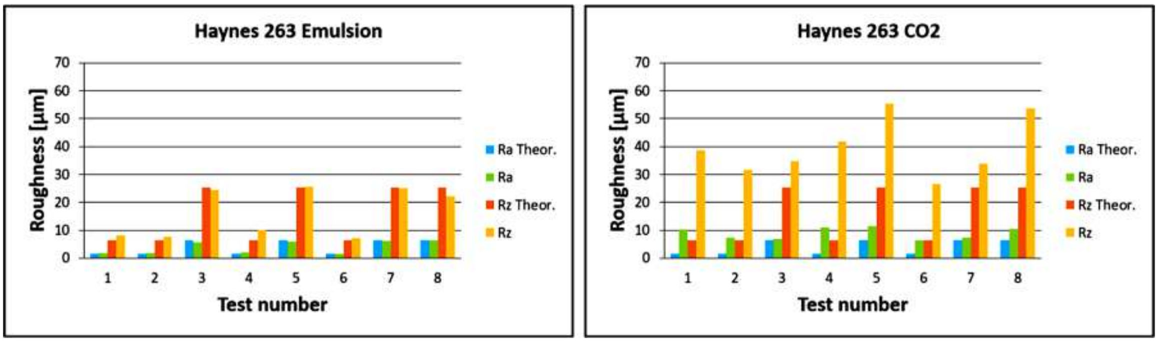

Fig. 8. Measured and theoretical roughness R_a, R_z (Haynes 263, emulsion and CO_2 conditions).

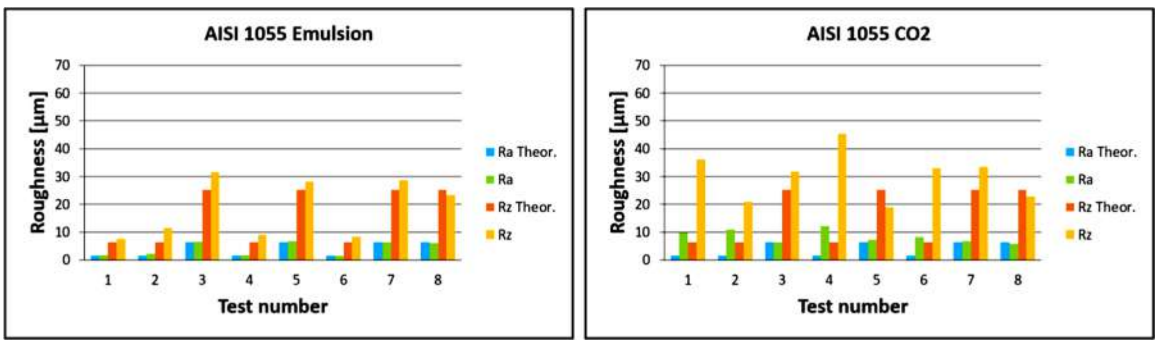

Fig. 9. Measured and theoretical roughness R_a, R_z (AISI 1055, emulsion and CO_2 conditions).

where inv[A] is the inverse matrix of [A] defined in Eq. 1.

The specific components of the cutting force are easily obtained from solving the corresponding systems for feeds taken in pairs. Tables A1–A6 in the Appendix show the obtained cutting coefficients for the three materials using both cooling alternatives. To build a reliable prediction model that accounts for any combination of feed, depth of cut and cutting speed, a polynomial fitting of the following type is proposed:

$$K = f\,(a_p,\, V_c) = A + B^*a_p + C^*V_c + D^*a_p{}^*V_c + E^*a_p{}^2 + F^*V_c{}^2 \tag{5}$$

This symmetric quadratic fitting is proposed for all the cases with subtle modifications in order to minimize errors between predicted and experimental results. Tables B1–B6 in Appendix B depict the subsequent fitting factors, A to F, for the specific cutting coefficient evaluation in the parameter window.

Figs. 10–13 represent the three-dimensional surface of the double variable fitting for superalloy materials. The variation of the corresponding specific cutting coefficients with the depth of cut and the cutting speed is shown. In addition, the graphs show the points considered for the measurement as well as their value and the error with respect to the model created. Sometimes the particular error of a coefficient can be high since the model consists of few terms and must be adapted to all the points, however the forces calculated through the model are a linear combination of the coefficients so the errors are minimized as will be seen finally.

Comparing Figs. 10 and 11, it can be seen that the errors of the coefficients between the models and the experimental data are greater with the use of CO_2 in the case of Inconel 718. The opposite occurs between Figs. 12 and 13 where the errors are greater in the machining of Haynes 263 using oil emulsion. This trend can be confirmed in Fig. 14 where the cutting forces on the Y-axis calculated from the coefficients of the models, taking intermediate cutting conditions, a_p = 0.5 mm, f = 0.3 mm/rev, V_c = 60 m/min (V_c = 300 m/min on steel) are shown.

Machining forces in Inconel 718 and Haynes 263 are very similar but with opposite effects depending on the coolant type used. It is interesting to see how the use of CO_2 in Inconel 718 is only favorable at high depths of cut and high speeds. In the case of Haynes 263, Fig. 14 shows a great margin in the use of CO_2. Even at low depths of cut, the use of CO_2 reduces the cutting force F_y at high speeds and feeds. For increasing depths of cut, the margin is progressively improved. In the case of AISI 1055 steel, the advantage of using CO_2 is clearly seen with the increase in cutting parameters. The forces on steel are obviously lower due to the nature of the material, but coolant effect is similar to that of Haynes 263.

It can be observed that at high cutting speeds the use of CO_2 is beneficial in all cases as the forces continue to decrease; however, the emulsion ceases to have any effect in the case of Haynes 263 and steel when the forces are stabilized.

The increased feed rate in the machining of Inconel 718 increases the cutting forces but keeps the forces produced with CO_2 above those of the emulsion, maintaining the difference between the two. In steel, there is a slight improvement with the use of CO_2 as the feed rate increases, but in the case of Haynes 263 the increase in feed rate greatly increases the forces with the use of emulsion with respect to the use of CO_2.

The inverse behavior with respect to the cutting forces and with respect to the errors of the coefficients, concerning both superalloys, can be related. The superalloys have a metallurgical composition whose properties offer a high resistance to thermal creep, but not all of them are equally suitable. Inconel 718 alloy is more susceptible to strain-age cracking than Haynes 263 and less ductile below 800 °C [30], so the type of lubrication used can affect their machining.

The difference in hardness between the two materials, which can be seen in Table 1, is explained by the microstructure. The usual hardening mechanism in nickel-based alloys is the formation of ductile secondary phase precipitates γ´ Ni_3(Ti, Al). Some authors studied how the presence of Niobium increases the hardness of superalloys with high iron content, such as Inconel 718, where it produces Ni_3Nb precipitates in a phase with higher thermal stability and lower ductility [31].

As described above, the cutting-edge angle is low in this type of

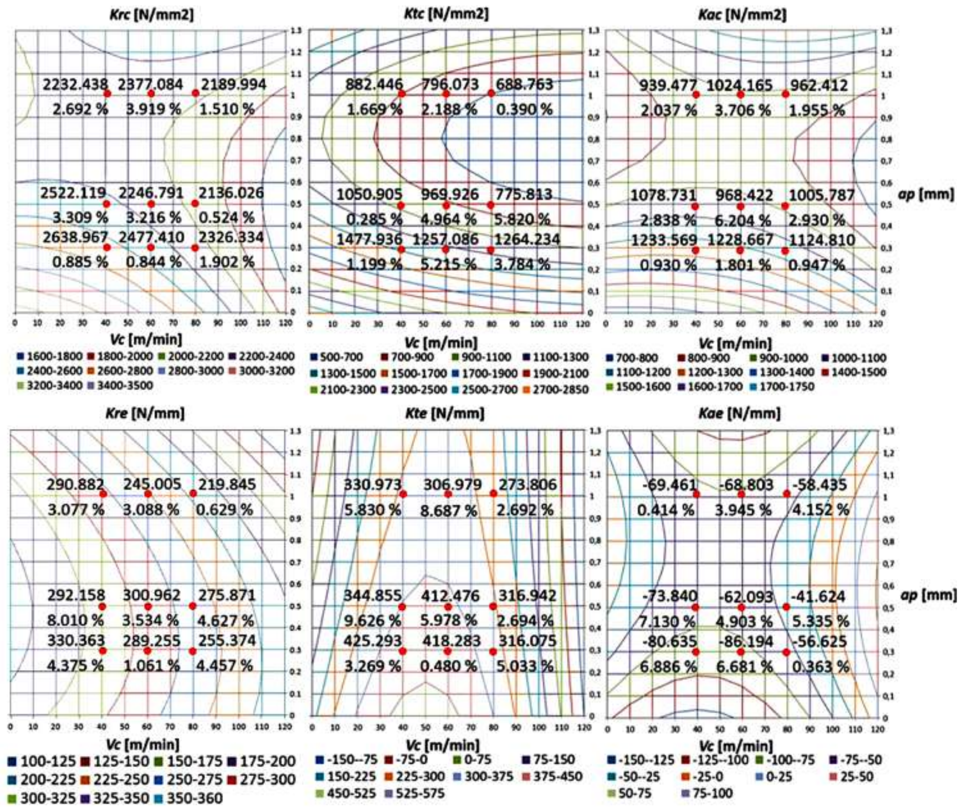

Fig. 10. Mapping of specific force coefficients and errors. Inconel 718 - oil emulsion.

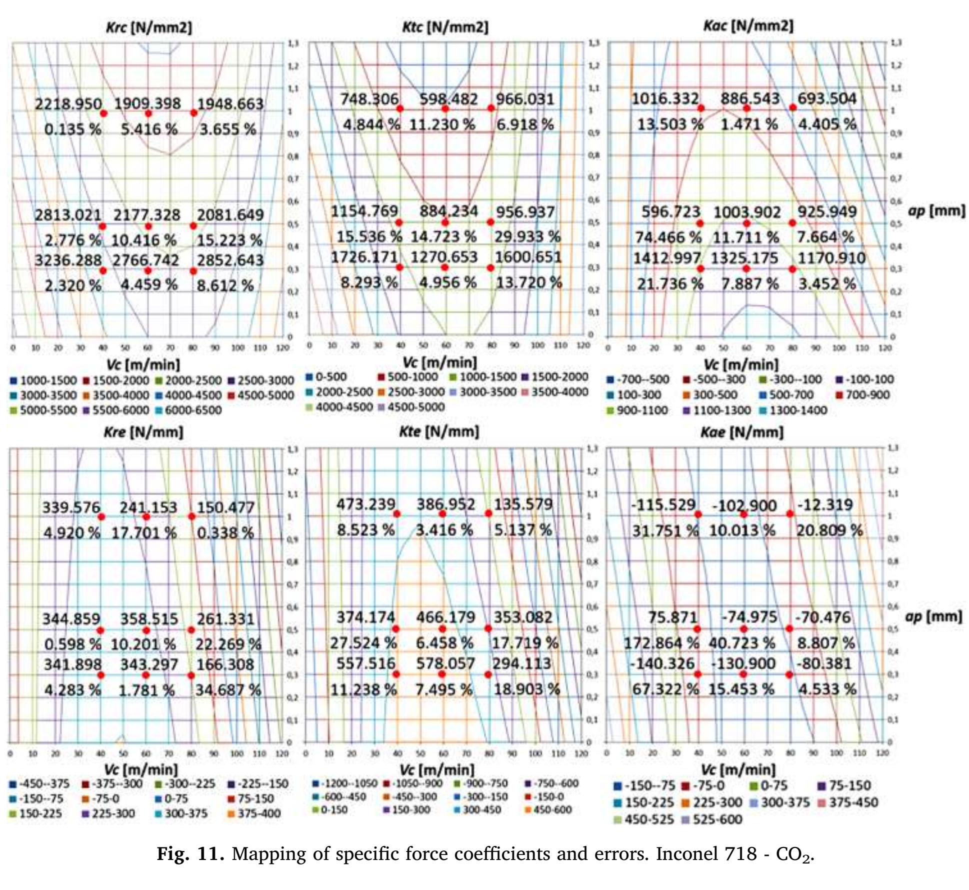

Fig. 11. Mapping of specific force coefficients and errors. Inconel 718 - CO_2.

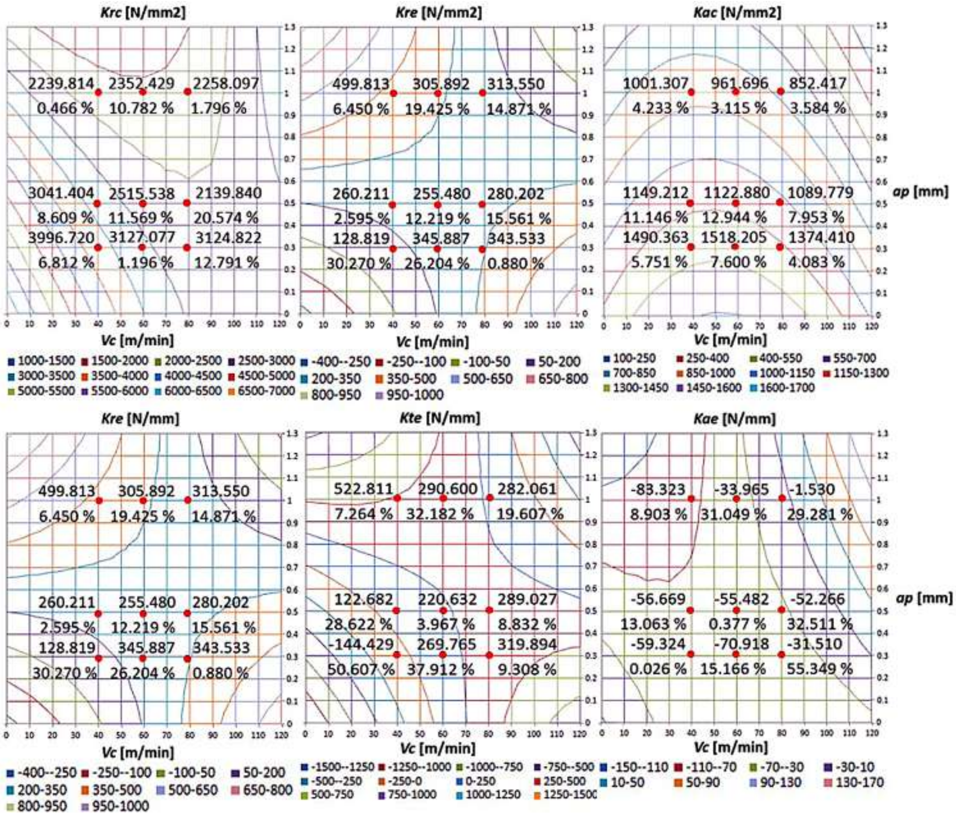

Fig. 12. Mapping of specific force coefficients and errors. Haynes 263 - oil emulsion.

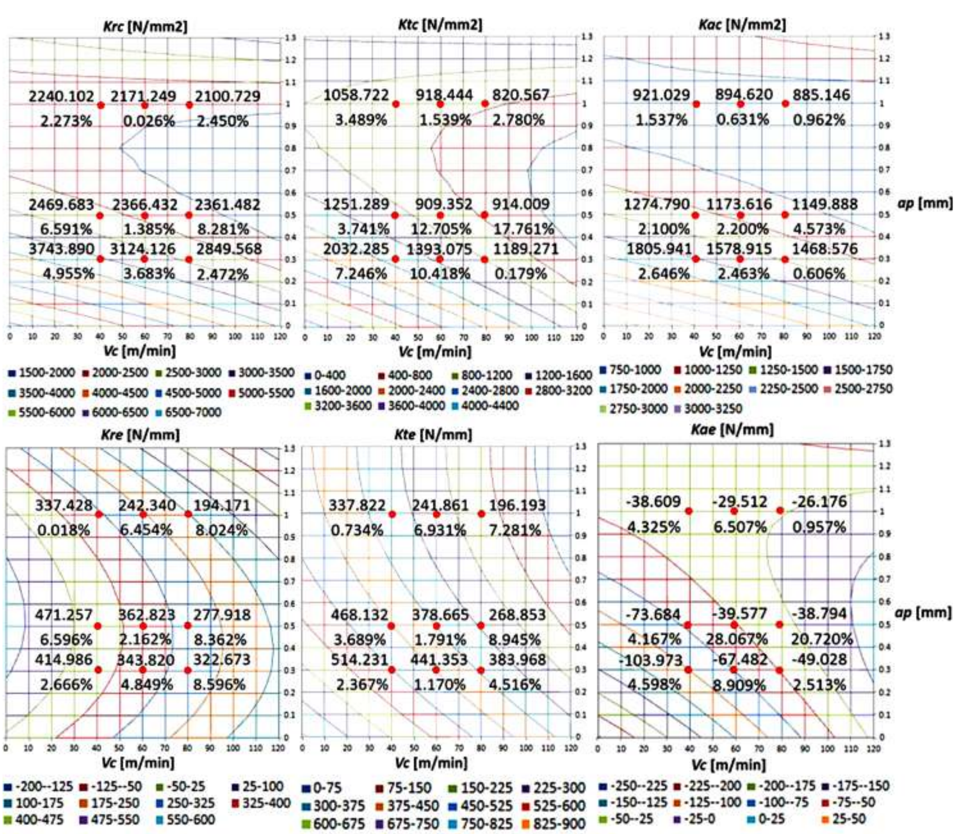

Fig. 13. Mapping of specific force coefficients and errors. Haynes 263 - CO_2.

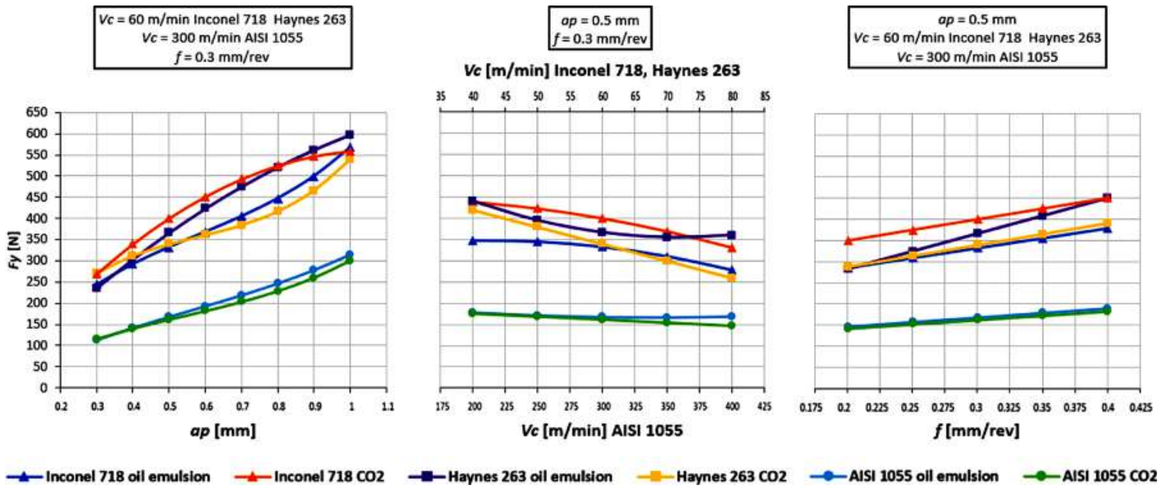

Fig. 14. F_y force trend as a function of a_p, V_c and f.

Fig. 15. 3D scanning of the inserts after machining. a. Inconel 718-oil emulsion; b. Haynes 263-oil emulsion.

turning ($\kappa_r = 30^{\circ}$). This produces a wide chip that must slide over a large surface of the insert, so the friction component can have a greater relative importance to the shear component.

The use of CO_2 produces a higher cutting force at low a_p than with the use of traditional emulsion, whose lubricating capacity decreases friction. But as a_p increases, edge length and friction increase. Haynes 263 high resistance to strain-age cracking allows it to resist the heat generated in machining with emulsion. Its ductility together with its low hardness increasing the contact between the tool and the chip and the forces increase considerably. The material adheres, forming a raised edge, as can be seen in Fig. 15b.

In the case of Inconel 718, the higher thermal stability, higher hardness and lower ductility result in less tool-chip contact. Fig. 15a shows the absence of material adhered to the insert. The lubricating action of the oil makes the use of emulsion in Inconel 718 more beneficial, so the use of CO_2 is more restricted and only at high a_p and V_c, in very hard working conditions. Hardness, low ductility and the non-lubrication conditions explain the dispersion in coefficient errors of Inconel 718 using CO_2, since they cause the lack of contact between the insert and the chip, avoiding a good repeatability of the friction forces data.

In AISI 1055, the addition of CO_2 hardens the material, but at the same time it tends to cools it. On the other hand, the emulsion lubricates the process and improves heat dissipation better than in the superalloys due to a higher thermal conductivity. There is a balance in both cooling methods in the way cutting forces are similar, although slightly favorable in the case of CO_2.

Therefore, machining forces have been obtained by means of a dynamometer in turning tests of aeronautical use alloys, with high nickel content, at different cutting parameters, in order to create models that describe the behaviour of the process compared to a steel alloy for conventional use. The procedure to obtain forces has been repeated using emulsion and CO_2 as coolants to know in which conditions each process is optimized. The force comparison between the two coolants reveals that the use of CO_2 is more favourable in the machining of Haynes 263 and AISI 1055 while in the machining of Inconel 718 the use of emulsion is preferable. In all three cases the transition between the use of emulsion to CO_2 becomes favourable with the increase of a_p and V_c.

Table 4
Validation results. Experimental and predicted forces and errors - Inconel 718.

Cutting parameters			Material	Oil emulsion			CO_2		
a_p [mm]	Vc [m/min]	f [mm/rev]	Inconel 718	F_X [N]	F_Y [N]	F_Z [N]	F_X [N]	F_Y [N]	F_Z [N]
0.3 0.5 1	**40 60 80**	**0.2 0.3 0.35 0.4**	**Average model error (%)**	**1.338**	**3.000**	**2.006**	**3.344**	**7.844**	**3.339**
Validation 1			**Exp. force**	703.9	381.3	−171.0	733.8	476.4	−205.8
0.6	**50**	**0.37**	**Model force**	691.6	418.0	−192.1	740.1	521.4	−218.4
			Error (%)	**1.756**	**9.634**	**12.301**	**0.853**	**9.453**	**6.131**
Validation 2			**Exp. force**	570.3	386.6	−184.4	557.8	396.5	−182.0
0.7	**70**	**0.25**	**Model force**	554.5	352.5	−174.9	531.6	417.5	−179.0
			Error (%)	**2.774**	**8.831**	**5.150**	**4.703**	**5.292**	**1.635**
Validation 3			**Exp. force**	808.6	482.3	−228.2	842.5	591.7	−280.7
0.85	**45**	**0.32**	**Model force**	847.4	503.3	−259.6	869.3	608.8	−287.8
			Error (%)	**4.797**	**4.352**	**13.783**	**3.185**	**2.903**	**2.543**

Table 5
Validation results. Experimental and predicted forces and errors - Haynes 263.

Cutting parameters			Material	Oil emulsion			CO_2		
a_p [mm]	Vc [m/min]	f [mm/rev]	Haynes 263	F_X [N]	F_Y [N]	F_Z [N]	F_X [N]	F_Y [N]	F_Z [N]
0.3 **0.5** **1**	**40** **60** **80**	**0.2** **0.3** **0.35** **0.4**	**Average model error (%)**	**7.829**	**9.681**	**8.316**	**2.012**	**3.765**	**3.801**
Validation 1			**Exp. force**	827.1	530.9	−219.6	749.2	446.9	−180.4
0.6	**50**	**0.37**	**Model force**	819.0	537.7	−203.3	743.6	447.5	−183.8
			Error (%)	**0.977**	**1.282**	**7.403**	**0.740**	**0.140**	**1.901**
Validation 2			**Exp. force**	625.9	394.4	−183.3	599.9	350.1	−157.2
0.7	**70**	**0.25**	**Model force**	640.5	409.9	−179.3	549.6	312.2	−155.2
			Error (%)	**2.330**	**3.909**	**2.201**	**8.384**	**10.840**	**1.213**
Validation 3			**Exp. force**	957.4	691.000	−313.0	881.8	533.4	−239.3
0.85	**45**	**0.32**	**Model force**	983.9	673.2	−302.3	854.7	530.8	−247.6
			Error (%)	**2.769**	**2.580**	**3.420**	**3.073**	**0.493**	**3.457**

Table 6
Experimental and predicted forces and errors - AISI 1055.

Cutting parameters			Material	Oil emulsion			CO_2		
a_p [mm]	Vc [m/min]	f [mm/rev]	Steel AISI 1055	F_X [N]	F_Y [N]	F_Z [N]	F_X [N]	F_Y [N]	F_Z [N]
0.3 **0.5** **1**	**200** **300** **400**	**0.2** **0.3** **0.35** **0.4**	**Average model error (%)**	**5.462**	**7.017**	**8.847**	**4.537**	**2.261**	**3.242**
Validation 1			**Exp. force**	453.5	201.3	−91.3	459.4	208.0	−93.2
0.6	**250**	**0.37**	**Model force**	455.1	213.4	−96.0	464.5	206.5	−95.3
			Error (%)	**0.360**	**6.015**	**5.142**	**1.114**	**0.711**	**2.275**
Validation 2			**Exp. force**	389.1	216.8	−102.1	372.0	180.1	−98.5
0.7	**350**	**0.25**	**Model force**	406.6	207.1	−108.3	364.9	183.7	−94.1
			Error (%)	**4.483**	**4.486**	**6.107**	**1.904**	**1.962**	**4.489**
Validation 3			**Exp. force**	550.1	282.2	−135.2	530.6	272.7	−126.5
0.85	**225**	**0.32**	**Model force**	581.8	276.2	−142.4	582.7	264.1	−135.1
			Error (%)	**5.765**	**2.108**	**5.344**	**9.828**	**3.151**	**6.841**

5. Validation

Once the specific cutting coefficients are calibrated, the theoretical cutting forces can be calculated and compared with the actual ones. To show the reliability of the models, three validations were performed in each case by taking cutting forces in turning tests and comparing them with the model predictions. Tables 4–6 summarise the actual and theoretical force data of the proposed validations, as well as the corresponding errors. In addition, the average error of the models with respect to the original force data obtained in the tests when combining the different parameters *ap*, *Vc* and *f* is given.

In the case of Inconel 718, Table 4 shows that the errors of forces, in general, are greater with the use of CO_2 than with the emulsion, as well as the errors in the coefficients. However, as explained above, in the case of Haynes 263 and AISI 1055, shown in Tables 5 and 6 respectively, the trend is reverted, with fewer errors observed with the use of CO_2. In general, among the random cases selected for the validation, good agreement was observed. However, the validations performed for Inconel cases were found less accurate comparing to Haynes and to AISI cases.

6. Conclusions

Recently, high-feed turning was proposed as a promising alternative to improve productivity with respect to traditional turning operations. Besides, heavy cases for aerospace turbines are usually made of low machinability materials and turning stage is a time-consuming task. There is a margin to reduce cycle times and high-feed turning can find here an important market niche.

This work addresses the modelling and prediction of cutting forces in high feed turning process with low machinability alloys. First, a mechanistic turning model with constant side cutting edge angle was proposed. Then, Nickel-Chrome superalloys -Inconel 718 and Haynes 263- were investigated and compared against the reference, AISI 1055 steel, using two cooling alternatives: oil emulsion and CO_2 cryogenic coolant. The model was put to work and verified. Some remarks are:

- The mechanistic model reflects well the behavior of the modelled A-type insert suggesting that neglecting the effect of the nose radius at the tool tip inside the model is justified. A very good agreement was found specially for AISI 1055 and Haynes 263, while, some problems inherent to Inconel 718 were found. This is indeed the most difficult-to-machine material and showed the greatest errors between predicted and measured mean force values. However, errors below 14% were found for all the verification tests.
- It has been observed that the F_x module is the largest, instead of F_y as in other processes. This is due to the reduced side cutting edge angle. The increase of *ap* and *f* increases the cutting forces, while V_c decreases them.
- Roughness can be predicted fairly accurately by estimating the

theoretical roughness where emulsion is used. In cases where CO_2 is used as a coolant, the roughness is considerably higher, due to the low lubricating power. The hardness of the material is closely related to the degree of roughness observed.

- For the turning of Inconel 718, oil emulsion was clearly found as the best option. However, for Haynes 263, a market niche can be opened for cryogenic cooling with CO_2 which is a technology with a good balance between technical and environmental (cleaner than oil emulsion) aspects. This can be a step forward towards reducing the environmental footprint over turbofans manufacturing processes. High feed turning combined with CO_2 cooling technique can satisfy productivity and sustainability.

Declaration of Competing Interest

The authors report no declarations of interest.

Acknowledgements

We are thankful to Excellence Groups of the Basque University IT1337-19, Spanish Ministry of Economy Project IB-RELIABLE (DPI2016-74845-R) and Elkartek PROCODA KK-2019/00004.

Appendix A. Set of obtained specific cutting coefficients for the different materials using oil emulsion and CO_2

Table A1
Specific cutting force components for Inconel 718 - oil emulsion.

a_p [mm]	*Vc* [m/min]	*Krc* [N/mm²]	*Kre* [N/mm]	*Ktc* [N/mm²]	*Kte* [N/mm]	*Kac* [N/mm²]	*Kae* [N/mm]
	40	2232.438	290.882	882.446	330.973	939.477	−69.461
1	**60**	2377.084	245.005	796.073	306.979	1024.165	−68.803
	80	2189.994	219.845	688.763	273.806	962.412	−58.435
	40	2522.119	292.158	1050.905	344.855	1078.731	−73.840
0.5	**60**	2246.791	300.962	969.926	412.476	968.422	−62.093
	80	2136.026	275.871	775.813	316.942	1005.787	−41.624
	40	2638.967	330.363	1477.936	425.293	1233.569	−80.635
0.3	**60**	2477.410	289.255	1257.086	418.283	1228.667	−86.194
	80	2326.334	255.374	1264.234	316.075	1124.810	−56.625

Table A2
Specific cutting force components for Inconel 718 - CO_2.

a_p [mm]	*Vc* [m/min]	*Krc* [N/mm²]	*Kre* [N/mm]	*Ktc* [N/mm²]	*Kte* [N/mm]	*Kac* [N/mm²]	*Kae* [N/mm]
	40	2218.950	339.576	748.306	473.239	1016.332	−115.529
1	**60**	1909.398	241.153	598.482	386.952	886.543	−102.900
	80	1948.663	150.477	966.031	135.579	693.504	−12.319
	40	2813.021	344.859	1154.769	374.174	596.723	75.871
0.5	**60**	2177.328	358.515	884.234	466.179	1003.902	−74.975
	80	2081.649	261.331	956.937	353.082	925.949	−70.476
	40	3236.288	341.898	1726.171	557.516	1412.997	−140.326
0.3	**60**	2766.742	343.297	1270.653	578.057	1325.175	−130.900
	80	2852.643	166.308	1600.651	294.113	1170.910	−80.381

Table A3
Specific cutting force components for Haynes 263 - oil emulsion.

a_p [mm]	*Vc* [m/min]	*Krc* [N/mm²]	*Kre* [N/mm]	*Ktc* [N/mm²]	*Kte* [N/mm]	*Kac* [N/mm²]	*Kae* [N/mm]
	40	2239.814	499.813	987.194	522.811	1001.307	−83.323
1	**60**	2352.429	305.892	1028.833	290.600	961.696	−33.965
	80	2258.097	313.550	1011.028	282.061	852.417	−1.530
	40	3041.404	260.211	2415.570	122.682	1149.212	−56.669
0.5	**60**	2515.538	255.480	1474.963	220.632	1122.880	−55.482
	80	2139.840	280.202	895.719	289.027	1089.779	−52.266
	40	3996.720	128.819	3580.234	−144.429	1490.363	−59.324
0.3	**60**	3127.077	345.887	1948.225	269.765	1518.205	−70.918
	80	3124.822	343.533	1939.608	319.894	1374.410	−31.510

Table A4
Specific cutting force components for Haynes 263 - CO_2.

a_p [mm]	Vc [m/min]	Krc [N/mm^2]	Kre [N/mm]	Ktc [N/mm^2]	Kte [N/mm]	Kac [N/mm^2]	Kae [N/mm]
	40	2240.102	337.428	1058.722	337.822	921.029	−38.609
1	**60**	2171.249	242.340	918.444	241.861	894.620	−29.512
	80	2100.729	194.171	820.567	196.193	885.146	−26.176
	40	2469.683	471.257	1251.289	468.132	1274.790	−73.684
0.5	**60**	2366.432	362.823	909.352	378.665	1173.616	−39.577
	80	2361.482	277.918	914.009	268.853	1149.888	−38.794
	40	3743.890	414.986	2032.285	514.231	1805.941	−103.973
0.3	**60**	3124.126	343.820	1393.075	441.353	1578.915	−67.482
	80	2849.568	322.673	1189.271	383.968	1468.576	−49.028

Table A5
Specific cutting force components for AISI 1055 - oil emulsion.

a_p [mm]	Vc [m/min]	Krc [N/mm^2]	Kre [N/mm]	Ktc [N/mm^2]	Kte [N/mm]	Kac [N/mm^2]	Kae [N/mm]
	200	1458.204	187.708	454.516	182.133	650.786	−19.004
1	**300**	1456.138	178.181	434.561	175.639	656.882	−18.287
	400	1404.718	206.150	364.560	233.111	668.320	−37.627
	200	1478.142	308.885	435.417	262.439	733.992	3.913
0.5	**300**	866.613	417.987	409.284	232.312	572.320	38.584
	400	1372.156	146.845	421.001	155.328	660.715	−12.955
	200	1593.932	188.084	641.113	181.647	810.940	−12.134
0.3	**300**	1567.003	153.837	611.388	183.685	733.690	3.756
	400	1665.177	217.269	537.465	255.080	886.068	−24.847

Table A6
Specific cutting force components for AISI 1055 - CO_2.

a_p [mm]	Vc [m/min]	Krc [N/mm^2]	Kre [N/mm]	Ktc [N/mm^2]	Kte [N/mm]	Kac [N/mm^2]	Kae [N/mm]
	200	1515.524	174.985	465.068	176.635	668.348	−15.814
1	**300**	1511.874	152.814	429.873	167.814	686.849	−23.044
	400	1377.657	142.216	429.618	158.378	612.500	−24.773
	200	1712.519	207.947	508.893	215.480	822.579	−18.988
0.5	**300**	1519.719	177.828	394.391	200.706	755.930	−22.094
	400	1238.107	144.877	373.117	170.007	602.481	−22.777
	200	1663.417	156.404	721.738	190.299	814.197	−25.229
0.3	**300**	1489.773	179.548	504.498	243.930	811.807	−34.289
	400	1617.960	147.363	498.797	209.062	846.927	−33.317

Appendix B

Table B1
Fitting terms for specific cutting force components. Inconel 718 - oil emulsion.

Fitting term	Krc [N/mm^2]	Kre [N/mm]	Ktc [N/mm^2]	Kte [N/mm]	Kac [N/mm^2]	Kae [N/mm]
A	3479.289	338.670	2823.217	206.020	1748.966	−96.615
B	−2506.197	89.603	−4049.525	−254.312	−2094.094	213.198
C	−5.001	−0.808	−11.200	11.025	0.731	−1.771
D	11.098	−0.412	1.360	1.220	4.721	−0.578
E	1180.015	−93.574	2454.447	48.507	1150.838	−127.508
F	−0.065	−0.002	0.039	−0.111	−0.041	0.022

Table B2
Fitting terms for specific cutting force components. Inconel 718 - CO_2.

Fitting term	*Krc* [N/mm^2]	*Kre* [N/mm]	*Ktc* [N/mm^2]	*Kte* [N/mm]	*Kac* [N/mm^2]	*Kae* [N/mm]
A	6138.650	111.358	4519.863	−295.225	255.486	416.074
B	−1658.485	8.081	−1800.118	118.924	19.994	−193.033
C	−88.380	11.182	−91.525	31.661	33.936	−15.768
D	7.703	−1.405	13.897	−5.186	−8.599	3.648
E	-	-	-	-	-	-
F	0.602	−0.117	0.686	−0.281	−0.256	0.114

Table B3
Fitting terms for specific cutting force components. Haynes 263 - oil emulsion.

Fitting term	*Krc* [N/mm^2]	*Kre* [N/mm]	*Ktc* [N/mm^2]	*Kte* [N/mm]	*Kac* [N/mm^2]	*Kae* [N/mm]
A	6850.676	−286.518	9363.297	−1248.340	1329.562	13.130
B	−3486.928	970.222	−5705.002	1764.651	−564.350	−115.716
C	−75.871	7.953	−160.118	26.299	10.788	−2.236
D	34.523	−13.550	62.856	−24.253	−1.810	2.301
E	-	-	-	-	-	-
F	0.338	0.005	0.802	−0.071	−0.103	0.015

Table B4
Fitting terms for specific cutting force components. Haynes 263 - CO_2.

Fitting term	*Krc* [N/mm^2]	*Kre* [N/mm]	*Ktc* [N/mm^2]	*Kte* [N/mm]	*Kac* [N/mm^2]	*Kae* [N/mm]
A	6645.396	464.929	4190.293	833.631	3158.395	−226.950
B	−9766.313	425.839	−6393.001	−554.358	−4371.976	286.913
C	−22.402	−2.981	−22.861	−4.062	−9.883	1.718
D	21.478	−0.988	18.401	0.226	9.553	−1.442
E	5347.096	−394.622	3402.888	209.503	2133.660	−107.915
F	-	-	-	-	-	-

Table B5
Fitting terms for specific cutting force components. AISI 1055 - oil emulsion.

Fitting term	*Krc* [N/mm^2]	*Kre* [N/mm]	*Ktc* [N/mm^2]	*Kte* [N/mm]	*Kac* [N/mm^2]	*Kae* [N/mm]
A	4234.922	−358.139	1058.057	315.769	1844.542	−271.830
B	−4234.625	1267.627	−1843.297	98.710	−1615.506	315.002
C	−11.704	2.089	0.257	−0.941	−4.723	1.450
D	−0.619	0.285	−0.066	0.174	−0.158	−0.037
E	3214.433	−1036.185	1236.757	−127.012	1112.514	−248.934
F	0.020	−0.004	−0.001	0.001	0.008	−0.003

Table B6
Fitting terms for specific cutting force components. AISI 1055 - CO_2.

Fitting term	*Krc* [N/mm^2]	*Kre* [N/mm]	*Ktc* [N/mm^2]	*Kte* [N/mm]	*Kac* [N/mm^2]	*Kae* [N/mm]
A	2302.802	85.451	1864.763	99.033	933.138	−23.085
B	−1058.775	238.843	−2021.333	−92.037	−821.592	107.802
C	−1.989	0.338	−4.819	1.072	1.133	−0.205
D	0.114	−0.079	1.275	−0.161	−0.195	−0.015
E	654.019	−170.454	1114.037	56.554	491.965	−68.774
F	0.001	−0.001	0.006	−0.002	−0.002	0.000

References

[1] Aerospace Engine, Application Guide. Sandvik; 2020.
[2] Polvorosa R, Suarez A, Lacalle L, Cerrillo I, Wretland A, Veiga F. Tool wear on nickel alloys with different coolant pressures: Comparison of Alloy 718 and Waspaloy. Journal of Manufacturing Processes 2017;26:44–56.
[3] Sadílek M, Čep R, Sadílková Z, Valicek J, Petřkovská L. Increasing tool life during turning with a variable depth of cut. Materials and Technologies 2013;47:199–203.
[4] Selaimia A-A, Yallese MA, Bensouilah H, Meddour IK, Khattabi R, Mabrouki T. Modeling and optimization in dry face milling of X2CrNi18-9 austenitic stainless steel using RMS and desirability approach. Measurement 2017;107:53–67.
[5] Tukora B, Szalay T. Real-time determination of cutting force coefficients without cutting geometry restriction. International Journal of Machine Tools and Manufacture 2011;51(12):871–9.
[6] Matsumura T, Tamura S. Cutting Force Model in Milling with Cutter Runout. Procedia CIRP 2017;58:566–71.
[7] Tsai MY, Chang SY, Hung JP, Wang CC. Investigation of milling cutting forces and cutting coefficient for aluminum 6060-T6. Computers & Electrical Engineering 2016;51:320–30.
[8] Altintas Y. Manufacturing Automation. Cambridge, MA: Cambridge University Press; 2000.
[9] Zhou JM, Persson H, Chen Z, M'Saoubi R, Gustafsson D, Bushlya V, Akujärvi V, Stahl JE, Peng R. Surface Characterization of AD730TM Part Produced in High Speed Turning with CBN tool. Procedia CIRP 2018;71:215–20.
[10] Denkena B, Grove T, Krödel A, Ellersiek L. Increased performance in high speed turning of Inconel 718 by laser structuring of PcBN tools. Procedia CIRP 2018;77:602–5.
[11] Chen Z, Zhou JM, Peng RL, M'Saoubi R, Gustafsson D, Palmert F, Moverare J. Plastic Deformation and Residual Stress in High Speed Turning of AD730^{TM} Nickel-based Superalloy with PCBN and WC Tools. Procedia CIRP 2018;71:440–5.
[12] Soo SL, Khan SA, Aspinwall DK, Harden P, Mantle AL, Kappmeyer G, Pearson D, M'Saoubi R. High speed turning of Inconel 718 using PVD-coated PCBN tools. CIRP Annals 2016;65(no. 1):89–92.
[13] Tian X, Zhao J, Yang H, Wang Z, Liu H. High-speed intermittent turning of GH2132 alloy with Si3N4/(W, Ti)C/Co graded ceramic tool. The International Journal of Advanced Manufacturing Technology 2019;100(1):401–8.
[14] Yılmaz B, Karabulut Ş, Güllü A. Performance analysis of new external chip breaker for efficient machining of Inconel 718 and optimization of the cutting parameters. Journal of Manufacturing Processes 2018;32:553–63.
[15] Suárez A, Veiga F, de Lacalle LNL, Polvorosa R, Wretland A. An investigation of cutting forces and tool wear in turning of Haynes 282. Journal of Manufacturing Processes 2019;37:529–40.
[16] Günay M, Korkmaz ME, Yaşar N. Performance analysis of coated carbide tool in turning of Nimonic 80A superalloy under different cutting environments. Journal of Manufacturing Processes 2020;56:678–87.
[17] Thakur DG, Ramamoorthy B, Vijayaraghavan L. Study on the machinability characteristics of superalloy Inconel 718 during high speed turning. Materials & Design 2009;30(no. 5):1718–25.
[18] Kamata Y, Obikawa T. High speed MQL finish-turning of Inconel 718 with different coated tools. Journal of Materials Processing Technology 2007;192–193:281–6.
[19] Rahman M, Seah WKH, Teo TT. The machinability of inconel 718. Journal of Materials Processing Technology 1997;63(1):199–204.
[20] Fujimaki S, Shibayama T, Hayasaka T, Shamoto E. Proposal of 'Curved-Profile Wiper Turning' for efficient, stable, and smooth finishing. Precision Engineering 2020;61:152–9.
[21] Karpuschewski B, Kundrák J, Varga G, Deszpoth I, Borysenko D. Determination of specific cutting force components and exponents when applying high feed rates. Procedia CIRP 2018;77:30–3.
[22] Khan SA, Ahmad MA, Saleem MQ, Ghulam Z, Qureshi MAM. High-feed turning of AISI D2 tool steel using multi-radii tool inserts: Tool life, material removed, and workpiece surface integrity evaluation. Materials and Manufacturing Processes 2017;32(6):670–7.
[23] Pereira O, Rodríguez A, Fernández-Abia AI, Barreiro J, de Lacalle LNL. Cryogenic and minimum quantity lubrication for an eco-efficiency turning of AISI 304. Journal of Cleaner Production 2016;139:440–9.
[24] Pereira O, Rodríguez A, Barreiro J, Fernández-Abia AI, de Lacalle LNL. Nozzle design for combined use of MQL and cryogenic gas in machining. International Journal of Precision Engineering and Manufacturing-Green Technology 2017;4(1):87–95.
[25] Behera BC, Alemayehu H, Ghosh S, Rao PV. A comparative study of recent lubri-coolant strategies for turning of Ni-based superalloy. Journal of Manufacturing Processes 2017;30:541–52.
[26] Klocke F, Krämer A, Sangermann H, Lung D. Thermo-Mechanical Tool Load during High Performance Cutting of Hard-to-Cut Materials. Procedia CIRP 2012;1:295–300.
[27] Pereira O, Urbikain G, Rodríguez A, Fernández-Valdivielso A, Calleja A, Ayesta I, de Lacalle LNL. Internal cryolubrication approach for Inconel 718 milling. Procedia Manufacturing 2017;13:89–93.
[28] Shaw MC. Metal Cutting Principles. London: Oxford University Press; 2020.
[29] Budak E, Ozlu E. Analytical Modeling of Chatter Stability in Turning and Boring Operations: A Multi-Dimensional Approach. CIRP Annals 2007;56(1):401–4.
[30] Rowe MD. Ranking the resistance of wrought superalloys to strain-age cracking. Welding Journal (Miami, Fla) 2006;85:27S–34S.
[31] Cozar R, Pineau A. Morphology of y' and y" precipitates and thermal stability of inconel 718 type alloys. Metallurgical Transactions 1973;4:47–59.